

Electromechanical Quantum Simulators

F. Tacchino^{+,1} A. Chiesa^{+,2,3} M. D. LaHaye^{,4} S. Carretta^{,2,*} and D. Gerace^{1,†}

¹*Dipartimento di Fisica, Università di Pavia, via Bassi 6, I-27100 Pavia, Italy*

²*Dipartimento di Scienze Matematiche, Fisiche e Informatiche, Università di Parma, I-43124 Parma, Italy*

³*Institute for Advanced Simulations, Forschungszentrum Jülich, 52425 Jülich, Germany*

⁴*Department of Physics, Syracuse University, Syracuse NY 13244-1130, USA*

Quantum simulators are one of the most appealing applications of a quantum computer. Here we propose a universal, scalable, and integrated quantum computing platform based on tunable qubits encoded in electromechanical nano-oscillators within a superconducting microwave circuit. It is shown that very high operational fidelities can be achieved in a minimal architecture where qubits are encoded in the anharmonic vibrational modes of mechanical nanoresonators, whose effective coupling is mediated by virtual fluctuations of an intermediate superconducting artificial atom. We explicitly show, by using realistic parameters, the digital quantum simulation of the transverse field Ising model as a paradigmatic example, displaying very large theoretical fidelities, and discuss its potential scalability to simulate more complex model Hamiltonians.

I. INTRODUCTION

Thanks to the constant development of superconducting circuits over the past decade^{1–3}, unprecedented progress is currently ongoing towards achieving a scalable platform for quantum information processing that is based on purely superconducting qubits encoding⁴. However, scalability requires fidelities that are presently incompatible with the relatively short coherence times of typical superconducting elements, even if remarkable progress has been made since the introduction of *transmon* qubits^{5,6}. For such reasons, several proposals have been putting forward the idea of developing hybrid quantum circuits, in which superconducting elements are efficiently and coherently coupled to other degrees of freedom with possibly longer coherence times⁷. Among recent approaches, a hybrid spin-photon qubit encoding has been proposed to partly overcome the limitations of superconducting transmon qubits^{8,9}. In a parallel effort, hybrid optomechanical devices have been proposed for quantum information processing, e.g., by using the mechanical degrees-of-freedom of semiconductor nanoresonators¹⁰, while hybrid electromechanical systems could be used as analog quantum simulators of the Anderson model¹¹. Within this context, it should be noted that hybrid quantum electromechanical systems have already been realized in superconducting circuits with a focus on investigating qubit-nanoresonator interactions, which could be utilized for quantum state manipulation, storage and measurement^{12–17}.

Motivated by such technological progress, we hereby envision a novel hybrid architecture based on electromechanical superconducting elements, where universal and scalable quantum computation could be performed. At difference with the existing literature, we propose to use anharmonic and tunable nanomechanical resonators (NRs) to encode and store the quantum information, while only virtual fluctuations of superconducting elements such as transmons are employed to perform two-qubit gates, making their T_2 time essentially irrelevant.

As model nanomechanical systems, we consider electromechanical nano-oscillators that are compatible with superconducting circuits, such as nanomembranes^{18,19}, nanotubes^{20,21}, and graphene sheets^{22–24}, which have been shown to display remarkably low damping and decoherence rates. In addition, large tunability of their resonance frequencies^{22,23,25,26} as well as their nonlinear properties^{26–29} has been already shown, making them an ideal playground for prospective quantum technology applications.

The set-up proposed in this Letter has at least two prominent features to be highlighted: (i) the intrinsic scalability, and (ii) the large degree of external control and local tunability through classical fields. In fact, external magnetic control of the transmon frequency can be envisioned as an additional tuning knob³⁰, which can be employed to further optimize the fidelity of specific operations. These features allow to achieve ultra-high theoretical fidelities of elementary single- and two-qubit gates, which is crucial to apply this platform to realize a quantum simulator, i.e. a system able to mimic the time evolution of a large class of targeted models, provided they can be mapped onto spin Hamiltonians^{31–33}. Several proposals have recently targeted the implementation of digital quantum simulators in superconducting circuits^{34–39}. Here we explicitly perform numerical simulations to show the actual performances of an electromechanical quantum simulator based on the building blocks described above. In particular, we show the remarkable fidelities that could be achieved for the simulation of the transverse field Ising model and of the XY spin Hamiltonian, which could serve as a basis for the implementation of the fermionic Hubbard model.

II. MODEL

The fundamental unit of our architecture is composed of a pair of electromechanical NRs mutually coupled to a nonlinear circuit element, here assumed to be a superconducting transmon. A schematic representation of this

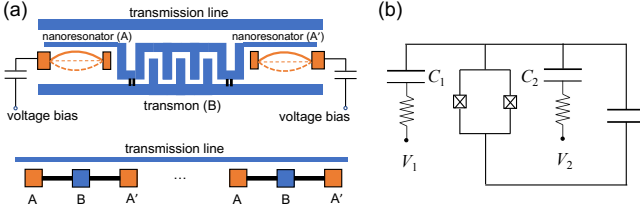


FIG. 1: (a) Schematic representation of the building block of the circuit architecture proposed in this work: two electromechanical oscillators mutually coupled through a transmon within a superconducting transmission line; each oscillator is tunable through either external voltage bias (the NR) or external magnetic fields (the transmon); the intrinsic scalability of this set-up is also sketched. (b) Analog circuit model of the elementary building block shown in (a).

elementary building block as well as the corresponding circuit model are shown in Fig. 1. Notice the straightforward scalability of this set-up according to a sequential repetition of the building block. A microwave superconducting resonator, which is not explicitly considered in the following, can be taken into account as a further element to be weakly coupled to the NR for ground state cooling¹⁸ (i.e., qubit initialization), while the transmon could also be employed for read out of each qubit state. This elementary unit can then be modeled through a second-quantized Hamiltonian, where the free mechanical resonators and the isolated transmon are described by ($\hbar = 1$)

$$H_0 = \sum_i \left[\omega_i b_i^\dagger b_i + H_{nl,i} \right] + \frac{\Omega}{2} \sigma_z, \quad (1)$$

with b_i (b_i^\dagger) representing bosonic annihilation (creation) operators, and $H_{nl,i}$ giving the necessary anharmonicity to isolate the two lowest energy levels of the NRs, where the qubits are encoded. The anharmonic contribution can be experimentally implemented through the use of intrinsic mechanical nonlinearities^{25,26}, or by using static external electric fields²⁶⁻²⁹. In order to keep our analysis simple, we will only require a shift of the lowest lying Fock energy levels, i.e. a diagonal term on the Fock basis, modeled by $H_{nl,i} = \beta b_i^\dagger b_i^\dagger b_i b_i$ (see App. A for details). The last term in Eq. (1) describes the transmon as a pure quantum two-level system⁵, σ_α ($\alpha = x, y, z$) representing the Pauli matrix.

The interaction between mechanical oscillators and transmon can be modeled as¹⁴

$$H_{int} = \sum_{i=1}^2 g_{i,x} (b_i + b_i^\dagger) \sigma_x + g_{i,z} (b_i + b_i^\dagger) \sigma_z. \quad (2)$$

It has been shown¹⁴ that $g_x \gg g_z$ in the transmon regime, and therefore the second term in Eq. (2) can be neglected (we will assume $g_{i,x} \equiv g_i$ in the following). We will set the electromechanical resonators frequencies below 100 MHz, while the transmon frequency will be set in the

2-10 GHz range. We notice that such an energy mismatch does not allow to employ the rotating wave approximation in Hamiltonian (2). Moreover, all the transmon excitations will only appear as virtual ones, while working with low-occupancy bosonic states. By a realistic choice of β , g_i and $\Delta_i = \omega_i - \Omega$, the dynamics is effectively restricted to the computational basis that we will be considering. Dissipation and pure dephasing effects are included in our model through Lindblad terms acting individually on the electromechanical NRs, i.e. $\mathcal{L}_i[\rho] = \gamma_i \mathcal{D}(b_i)[\rho] + \gamma_{i,d} \mathcal{D}(b_i^\dagger b_i)[\rho]$, and on the transmon, i.e. $\mathcal{L}_{TR}[\rho] = \gamma_{TR} \mathcal{D}(\sigma_-)[\rho] + \gamma_{TR,d} \mathcal{D}(\sigma_z)[\rho]$, respectively, where $\mathcal{D}(a)[\rho] = a\rho a^\dagger - 0.5\{a^\dagger a, \rho\}$.

An effective Hamiltonian can be derived by resorting to second order perturbation theory and by restricting to the portion of the total Hilbert space in which the transmon is in its ground state (details are provided in App. B), which describes the relevant dynamics of the pair of qubits restricted to the computational basis $\{|00\rangle, |10\rangle, |01\rangle, |11\rangle\}$:

$$H_{eff} = \sum_{i=1}^2 \left(\frac{\lambda_i}{2} \sigma_z^i \right) + \frac{\Gamma}{8} (\sigma_x^1 \sigma_x^2 + \sigma_y^1 \sigma_y^2) + \text{const.} \quad (3)$$

where the σ^i are Pauli operators in the computational basis of the NRs, λ_i are single-qubit energy shifts (i.e., transmon-induced frequency renormalizations, see App. B) and the effective XY coupling constant reads

$$\Gamma = \frac{4g_1 g_2 \Omega (\omega_1^2 + \omega_2^2 - 2\Omega^2)}{(\Omega^2 - \omega_1^2)(\Omega^2 - \omega_2^2)}. \quad (4)$$

We will use this H_{eff} as the reference model to understand the behavior of the real system, for which we numerically solve the full model above.

III. SINGLE AND TWO-QUBIT GATES

One of the key ingredients to perform single and two-qubit gates is the dynamical tuning of ω_1 and ω_2 . This can be achieved by using external static and modulated electric fields, i.e. electrostatic potential energies V , which can locally act on a single NR as already shown experimentally^{22,23,25,26}. In the idle configuration, the two NRs are significantly detuned: $|\omega_1 - \omega_2| \gg \Gamma$, thus switching off the interaction term appearing in Eq. (3). Hence, the two qubits are decoupled and independent rotations of each of them can be implemented. The use of a high-frequency transmon helps improving the two qubits decoupling.

In particular¹⁰, single qubit R_z -rotations can be performed by shifting the NRs oscillation frequency for the amount of time required to add the desired phase to the $n_i = 1$ component of the wave-function.

Other single-qubit rotations are obtained by an oscillating transverse field keeping a definite phase relationship with the quantum mechanical evolution of the system. Indeed, by choosing $H_i^{xy}(t) = V^{xy}(t)(b_i + b_i^\dagger)$, with

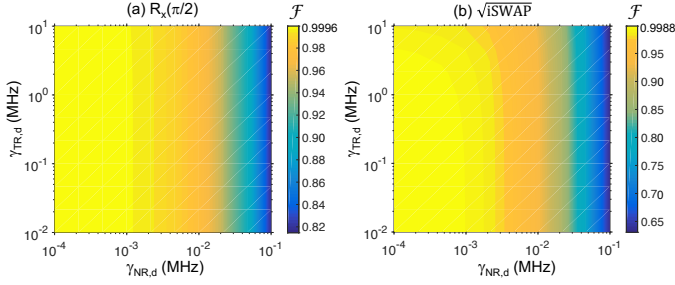


FIG. 2: (a) Fidelity of a single qubit x -rotation by a $\pi/2$ angle, and (b) fidelity of the two-qubit \sqrt{i} SWAP gate, as functions of the pure dephasing rates of the electromechanical resonators and the transmon, respectively. For the two-qubits gate, we assume $\gamma_{1,d} = \gamma_{2,d} = \gamma_{NR,d}$; all the other simulation parameters are reported in the text.

$V^{xy}(t) = \Theta_{t_0}(\delta t) V_0^{xy} \cos(\omega_i t + \theta)$ one can achieve either R_x^i ($\theta = 0$) or R_y^i ($\theta = \pi/2$) rotations. The total rotation angle equals the area under the pulse modulating the oscillation, i.e. $\phi_{xy} = -\int dt V_0^{xy} \Theta_{t_0}(\delta t)^{41}$.

Our setup can also straightforwardly implement the two-qubit entangling gate known as \sqrt{i} SWAP, described by the unitary matrix

$$U_{\sqrt{i}\text{SWAP}} = \begin{pmatrix} 1 & 0 & 0 & 0 \\ 0 & 1/\sqrt{2} & i/\sqrt{2} & 0 \\ 0 & i/\sqrt{2} & 1/\sqrt{2} & 0 \\ 0 & 0 & 0 & 1 \end{pmatrix} \quad (5)$$

This gate is obtained by tuning the qubits to resonance $\omega_i \rightarrow \omega'_i = \omega_i + \xi_i$ such that $\omega'_1 = \omega'_2$, thus activating the effective interaction term in Eq. (3). Indeed, the dynamics induced by the XY interaction in Eq. (3) corresponds to a \sqrt{i} SWAP for a proper choice of the interaction time $\tau = \pi/|\Gamma|$, as we show in App. C. The transmon-mediated interaction should then be turned off by bringing back the two NRs to their original frequencies⁴². Together with single-qubit rotations, this constitutes a universal set of quantum operations. A further tuning knob of the present set-up is the possibility of dynamically tuning the transmon frequency by varying an external magnetic flux, which allows to considerably shorten the required gating time (see Appendix for details).

The density matrix master equation describing the full system is written as

$$\partial_t \rho = i[\rho, \hat{H}_{tot}(t)] + \mathcal{L}_{TR}[\rho] + \sum_i \mathcal{L}_i[\rho], \quad (6)$$

where $\hat{H}_{tot}(t) = \hat{H}_0 + H_{int} + \hat{H}(t)$, and $H(t)$ includes all the time-dependent frequency shifts that are necessary to implement the gates. Eq. (6) is numerically integrated, in the interaction picture, by using a standard Runge-Kutta algorithm. A few representative examples of simulated single and two-qubit gates, together with a graphical description of the required external pulses, are shown in App. C. Here we report the computed fidelity of illustrative single- and two-qubit operations in

the presence of the main dissipation parameters of the model. As usual⁴³, the fidelity of a given gate is defined as $\mathcal{F} = \sqrt{\langle \psi | \rho | \psi \rangle}$, where ψ is the ideal target state and ρ is the density matrix evolved through Eq. (6). Realistic parameters for the hybrid circuit are assumed in all the simulations, such as: $\omega_1/2\pi = 85$ MHz and $\omega_2/2\pi = 75$ MHz (idle configuration), $\beta/2\pi = 3$ MHz (a conservative assumption²⁹), $\Omega/2\pi$ is tuned from 10 GHz (in idle configuration) down to 2.5 GHz (when performing two-qubit gates), $g_1 = g_2 = 2\pi \cdot 6$ MHz, $\gamma_1 = \gamma_2 = 2\pi \cdot 50$ Hz, $\gamma_{TR}/2\pi = 100$ kHz. We also tested the effects of non-negligible thermal occupation of the nanomechanical modes (i.e., non perfect ground state cooling), showing that it does not appreciably affect the gate performances with our protocol (see App. D). Finally, we checked that bosonic occupancies $n_i > 1$ do not occur throughout the whole gate dynamics.

As benchmark operations, we show in Fig. 2 the calculated fidelity of a single qubit R_x^1 -rotation with $\phi_x = \pi/2$ and of the \sqrt{i} SWAP gate, respectively, as a function of the pure dephasing rate (i.e., the reciprocal of the coherence time) for both the NRs and the transmon, respectively⁴⁴. We immediately notice a very weak dependence of \mathcal{F} on $\gamma_{TR,d}$ and, as it could be expected, a more sensitive dependence on $\gamma_{NR,d}$. In particular, it is worth reminding that a value of $\gamma_{NR,d}/2\pi \simeq 100$ kHz is utterly pessimistic for most of the electromechanical NRs, in particular nanomembranes and nanotubes, where total linewidths rather in the 0.1 – 1 kHz range have been experimentally probed^{21–23}. The most remarkable and clear-cut message to be drawn from these results is that, as intuitively expected from the virtual nature of transmon excitations participating in the gating, our scheme is intrinsically robust against transmon decoherence. Indeed, the results look practically insensitive to an increase of more than two orders of magnitude in $\gamma_{TR,d}$ from the most optimistic but still realistic⁶ value (i.e., $\gamma_{TR,d}/2\pi = 10$ kHz, corresponding to a transmon T_2 time of 100 μ s), for both single- and two-qubit gates.

IV. DIGITAL QUANTUM SIMULATIONS

The remarkable fidelities shown in the last Section for the elementary single and two-qubit gates are a crucial requirement for scaling up the quantum computation, e.g. to build a quantum simulator involving a long sequence of concatenated gates³². Here we tested the performances of a realistic proof-of-principle *digital* quantum simulation of illustrative models mapped onto spin-type Hamiltonians. This is done in analogy to previous works^{34,36,40}, by decomposing the time-evolution operator up to the instant t into the product of N terms, each evolving for short time intervals $\tau = t/N$, also named Trotter steps³¹. For sufficiently small τ , different terms of the target Hamiltonian commute, thus allowing us to decompose the target evolution into a sequence of quantum gates. In fact, we hereby focus on spin-type Hamiltonians since

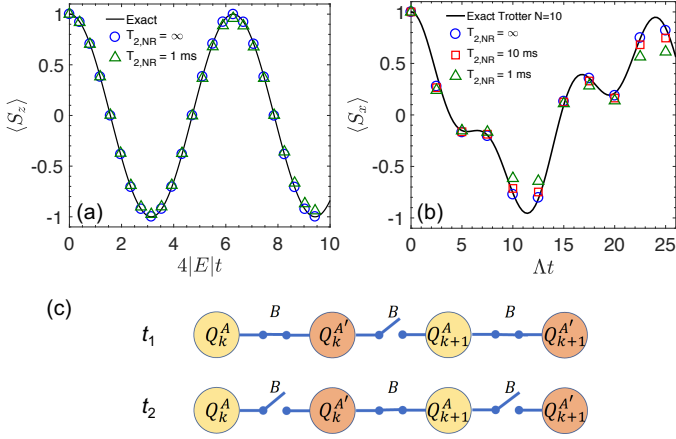


FIG. 3: (a) Exact time evolution of the total magnetization of a $S = 1$ system (full line) undergoing oscillations between opposite polarized states (describing, e.g., quantum tunneling across an anisotropy barrier), compared to the digital quantum simulation of the target Hamiltonian (7) for infinite and finite T_2 time of the electromechanical qubits, respectively (points). (b) Exact Trotter evolution ($N = 10$) of the total x -polarization in the model Hamiltonian (8) (full line), compared to the corresponding quantum simulation for different values of the qubits T_2 time (points). (c) Schematic illustration of the possible parallelization of the set-up utilizing 1D transmon-NR qubit chains, where next-neighbor gate sequences can be applied in parallel first on $A'A$ and then on AA' pairs of neighboring qubits. Here we show the transmon-NR chain at two different instances in time, t_1 and t_2 : at each instance a different combination of transmons (indicated by B) is utilized to switch on the effective qubit-qubit interactions in targeted qubit pairs.

most models of physical interest can be mapped onto a combination of local operators only involving one $\mathcal{H}_\alpha^{(1)}$ and two-body $\mathcal{H}_\alpha^{(2)}$ spin-terms, and the time evolution of these terms can be efficiently simulated through a proper sequence of one- and two-qubit gates. Indeed, the time evolution induced by $\mathcal{H}_\alpha^{(1)} \propto \sigma_\alpha^i$ directly corresponds to single-qubit rotations R_α^i . Conversely, two-body terms of the form $\mathcal{H}_\alpha^{(2)} \propto \sigma_\alpha^1 \sigma_\beta^2$ can be obtained by combining the XY evolution given by the second term in Eq. (3) with single qubit rotations (as explicitly reported in App. E). In the following results, we assumed $\gamma_{TR,d}/2\pi = 100$ kHz as realistic transmon dephasing rate, and checked the performances for different values of the nanomechanical qubits T_2 times.

As a first example, we show in Fig. 3(a) the quantum simulation of a spin-1 Hamiltonian initialized in a fully polarized eigenstate and experiencing tunneling of magnetization⁴⁵. The simulation of Hamiltonians involving $S > 1/2$ spins can be performed by encoding the state of each spin- S into that of $2S$ qubits. The target $S = 1$ Hamiltonian in this case reads

$$\mathcal{H}_{S1} = DS_z^2 + E(S_x^2 - S_y^2). \quad (7)$$

By considering the total spin as a combination of two

$1/2$ spins, $S_\alpha = s_{\alpha,1} + s_{\alpha,2}$, the mapped Hamiltonian $\mathcal{H}_{S1} = 2Ds_{z,1}s_{z,2} + 2E(s_{x,1}s_{x,2} - s_{y,1}s_{y,2})$ results in a sum of two body-terms that can be easily implemented in our platform. In particular, the evolution induced by $s_{x,1}s_{x,2} - s_{y,1}s_{y,2}$ is obtained by two $R_y(\pi)$ rotations on one of the two qubits, preceding and following the two-qubit evolution provided by H_{eff} (App. E). The exact time evolution of the total magnetization, $\langle S_z \rangle$, is compared in fig. 3(a) to a digital quantum simulation of $\tilde{\mathcal{H}}_{S1}$ with our electromechanical set-up, either for $\gamma_{NR,d} = 0$ or $\gamma_{NR,d}/2\pi = 1$ kHz. The overall quantum simulation works very well with an average fidelity $\mathcal{F} = 0.999$ for $\gamma_{NR,d} = 0$ and $\mathcal{F} = 0.988$ for $\gamma_{NR,d}/2\pi = 1$ kHz, respectively.

As a further test, Fig. 3(b) reports the digital quantum simulation of the total magnetization along x , i.e. $\langle S_x \rangle = \text{Tr}[\rho(s_{x,1} + s_{x,2})]$ ⁴⁶, for the transverse field Ising model of two $1/2$ spins, which reads

$$\mathcal{H}_{TIM} = \Lambda s_{x,1}s_{x,2} + b(s_{z,1} + s_{z,2}), \quad (8)$$

where we set $\Lambda = 2b = \Gamma$ for the specific simulation in Figure. Notice that the computation of each point in Fig. 3(b) (with $N = 10$ Trotter steps) requires the sequential concatenation of 20 two-qubit gates and 40 single-qubit rotations (each one operated in parallel on both qubits). Although this makes the simulation much more demanding, the fidelity is already 0.90 for $\gamma_{NR,d}/2\pi = 1$ kHz, which steeply increases to 0.96 if a more optimistic $\gamma_{NR,d}/2\pi = 100$ Hz is assumed. The latter result is especially noteworthy if one considers the total computational time required for the longest sequence of gates (i.e., corresponding to the last point in the Figure), which is about $150 \mu\text{s}$. This confirms the robustness and potential strength of the quantum computing platform introduced in this work.

In addition, by exploiting generalized Jordan-Wigner transformations to map fermionic into spin operators^{47,48}, it is possible to simulate many-body fermionic systems. In particular, our effective qubit-qubit interaction already implements a XY model, which is the essential building-block in the simulation of hopping processes in fermionic Hamiltonians³⁶. As a final comment we highlight the straightforward parallelization of this set-up, which could be accomplished through the fabrication of 1D transmon-NR arrays, in which each mechanical qubit is coupled to two adjacent transmons, as schematically represented in Fig. 3c. The targeted selection of parallel qubit pairs of the array could be implemented using fast voltage pulses from on-chip single-flux quantum (SFQ) circuitry, which is currently being developed for superconducting qubit architectures³⁰. The array and the pulse circuitry could be engineered using multilayer lithographic techniques, such as silicon *vias* and flip-chip stacks³. Notice that this possibility constitutes a major advantage of our proposed electromechanical set-up towards scalability, in particular as compared to alternative approaches where the two-qubit interactions are mediated by a single-mode resonator^{10,34}.

V. SUMMARY

In conclusion, we have proposed a scalable architecture to realize an electromechanical digital quantum simulator, based on state-of-the-art technology. Qubits are encoded in the anharmonic vibrational modes of mechanical nanoresonators, whose coupling is mediated by virtual excitations of an auxiliary transmon and can be switched on and off by tuning their resonance frequency. We have shown that the fidelity of elementary gates is practically unaffected by the transmon decoherence and remains remarkably high even with the inclusion of realistic values of the nanoresonators decoherence rates. These elementary gates are concatenated into quantum simulation algorithms and very good results are found for the implementation of non-trivial models, such as the transverse field Ising model and the XY model.

VI. ACKNOWLEDGEMENTS

This work was partly funded by the Italian Ministry of Education and Research (MIUR) through PRIN Project 2015 HYFSRT “Quantum Coherence in Nanostructures of Molecular Spin Qubits”. A. C. acknowledges financial support from “Fondazione Angelo Della Riccia”.

⁺ These authors contributed equally to this work.

Appendix A: Model of nanomechanical resonators anharmonicity

A certain degree of anharmonicity is the essential ingredient that allows a faithful encoding of information on the ground and first excited levels of each nano-electromechanical resonator. In our theoretical description we assumed a very simple model for the non linear contribution to the energy spectrum: indeed, a diagonal shift of the $|1\rangle \leftrightarrow |2\rangle$ transition with respect to $|0\rangle \leftrightarrow |1\rangle$ (in the Fock number basis representation of each qubit) already contains all the relevant features, while keeping the description easy to understand and analytically transparent. Here we compare this simplified description with a more realistic and commonly used model of anharmonic mechanical oscillators, with the aim of better clarifying the physical properties and parameters that are required from our nano-electromechanical devices.

From the perspective of the total bosonic Hilbert space (*i.e.* without truncation on the maximum number $n_{1,\max}$ and $n_{2,\max}$ of allowed excitations in each resonator), the diagonal non linearity model can be written as

$$H_{nl,diag} = Ub^\dagger b^\dagger bb \quad (A1)$$

On the other hand, a widely accepted model for non linear nanomechanical resonators is rather of the form

$$H_{nl} = U(b^\dagger + b)^4 \propto \hat{x}^4 \quad (A2)$$

As a first step in comparing the two situations, we will now show that the model that we adopted in the paper, given the same parameter U in the range of interest, underestimates the degree of required non linearity, *i.e.* it predicts a smaller shift $\delta = \omega_{21} - \omega_{10}$, with respect to (A2). This is easily seen in Fig. 4, where we compute δ by performing a numerical diagonalization of both models, after adding the free Hamiltonian $H_0 = \omega b^\dagger b$ and setting $n_{\max} = 10$. In the plot, U and δ are both expressed as fractions of the bare frequency of the oscillator ω . As it can easily be seen, in the range that corresponds to the region of interest for our purposes ($U/\omega \leq 0.1$), the model Hamiltonian (A1) is always quite conservative.

In addition to the eigenvalues, we also compared the eigenvectors corresponding to the first three energy levels (namely the computational basis plus the first extra level) for the two models. In this case, we selected the parameter U in two different ways such that the gap, δ , is the same both for $H_{nl,diag}$ and H_{nl} , such that $\delta = 2U = 6$ MHz. The two bare frequencies were assumed as $\omega_1 = 85$ MHz and $\omega_2 = 75$ MHz, corresponding to the values used in the simulations shown in the main text. The following table summarizes the fidelity, f , of the eigenvalues $|n\rangle_{nl}$ obtained from (A2) as compared to the corresponding bare Fock state, $|n\rangle$.

n	$f(\omega = \omega_1)$	$f(\omega = \omega_2)$
1	0.9996	0.9995
2	0.9971	0.9963
3	0.9899	0.9872

By using the $|n\rangle_{nl}$ states as elements of the computational basis, the very same protocol machinery that we presented in the paper can be used to implement single-qubit rotations and the \sqrt{i} SWAP gate. Indeed, electrical pulses can still be used to tune the fundamental transition frequency, ω_{01} , for both oscillators, thus bringing them to resonance when needed. Moreover, the operators b_i and b_i^\dagger promote transitions between the new eigenvectors, albeit with a slightly different matrix element $X_{kl} = \langle k|b|l\rangle$, as summarized in the following table.

X_{kl}	Fock states	$ n\rangle_{nl}$ for $(\omega = \omega_1)$	$ n\rangle_{nl}$ for $(\omega = \omega_2)$
X_{01}	1	1.0005	1.0007
X_{12}	$\sqrt{2}$	1.4170	1.4179

The Hamiltonian (A2) only couples Fock states differing by an even number of excitations. This means that $|n\rangle_{nl}$ and $|n+1\rangle_{nl}$ are still orthogonal to each other, since they are superpositions of even or odd Fock states only, namely eigenvectors of the parity operator on the Fock basis belonging to different eigenspaces. As a consequence, the matrix element X_{nn} vanishes. The same is not true for $X_{n(n+2)}$, meaning that b_i and b_i^\dagger could in principle promote $|0\rangle_{nl} \leftrightarrow |2\rangle_{nl}$ transitions outside the computational basis (*e.g.* during the single qubit xy rotations). However, in our protocol this effect remains negligible in view of the large energy gap between the two eigenstates.

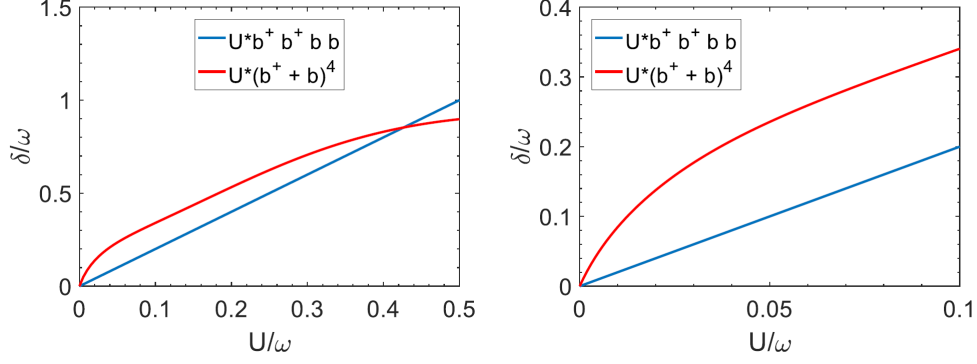


FIG. 4: Comparison between two possible models for non linearity of the nanoresonators. Panel on the right focuses on the region of interest for our setup.

In conclusion, the only significant consequence that we must keep into account is the rescaling of the coupling elements $g_i \rightarrow g_i X_{xy}$ (note that, in principle, this is specific for every transition) and the shortening, by a factor X_{01} , of the time required for the single qubit xy rotations. Numerical simulations of individual gates within this framework show behaviors and fidelities which are very close (the difference is below 0.1%) to the simplified case that we adopted.

Appendix B: Derivation of the effective qubit-qubit interaction

We provide here a detailed derivation of the effective Hamiltonian describing the interaction between the two qubits, mediated by virtual fluctuations of the interposed

transmon. This is obtained by considering

$$H_{int} = \sum_{i=1}^2 g_{i,x} (b_i + b_i^\dagger) \sigma_x \quad (B1)$$

as a weak perturbation with respect to

$$H_0 = \sum_{i=1,2} [\omega_i b_i^\dagger b_i + \beta b_i^\dagger b_i^\dagger b_i b_i] + \frac{\Omega}{2} \sigma_z. \quad (B2)$$

This condition is ensured, provided that $g_i \ll \Delta_i = \omega_i - \Omega$. Then we eliminate the transmon degrees of freedom by second order expansion and restrict to the two-qubit computational basis, where the transmon is frozen in its ground state. In this subspace, the matrix elements of the effective Hamiltonian are given by:

$$\begin{aligned} \langle \mu\nu | \tilde{H}_{eff} | \mu'\nu' \rangle &= \frac{1}{2} \sum_{m_1, m_2} \langle n_1 \downarrow n_2 | H_{int} | m_1 \uparrow m_2 \rangle \langle m_1 \uparrow m_2 | H_{int} | n'_1 \downarrow n'_2 \rangle \\ &\times \left[\frac{1}{\omega_1(n_1 - m_1) + \omega_2(n_2 - m_2) - \Omega} + \frac{1}{\omega_1(n'_1 - m_1) + \omega_2(n'_2 - m_2) - \Omega} \right]. \end{aligned} \quad (B3)$$

Here $|n_1 \sigma n_2\rangle$ are states in the full Hilbert space, with n_i being the bosonic occupation of each nonoresonator mode and $\sigma = \downarrow (\uparrow)$ indicating the ground (excited) state of the transmon. Conversely, \tilde{H}_{eff} operates in the 2-qubits Hilbert subspace, spanned by the computational basis $|\mu\nu\rangle$, with $\mu, \nu = 0, 1$. The sum runs over all the states with $\sigma = \uparrow$ (excited transmon). Finally, \tilde{H}_{eff} is decomposed in terms of Pauli operators σ_α^i . We report here the form it takes if bosonic states up to $m_i = 2$ are included:

$$\tilde{H}_{eff} = \sum_{i=1}^2 \left(\frac{\lambda_i}{2} \sigma_z^i \right) + \frac{\Gamma}{4} \sigma_x^1 \sigma_x^2 + \text{const.}, \quad (B4)$$

where

$$\Gamma = \frac{4g_1 g_2 \Omega (\omega_1^2 + \omega_2^2 - 2\Omega^2)}{(\Omega^2 - \omega_1^2)(\Omega^2 - \omega_2^2)} \quad (B5)$$

is the effective coupling, while

$$\lambda_i = \frac{-2g_i^2 (\Omega^2 + \omega_i (2\beta + \Omega))}{(2\beta + \Omega + \omega_i)(\Omega^2 - \omega_i^2)} \quad (B6)$$

are single-qubit energy shifts (corresponding to a renormalization of the qubit frequencies). Notice that \tilde{H}_{eff} was obtained while truncating bosonic occupancy up to 2, and it was restricted to the computational basis only

afterwards.

In order to get rid of the frequency renormalization induced by the transmon, we shift the bare frequencies ω_i by an amount $-\lambda_i$ throughout the whole gating dynamics. From the theoretical point of view, this detuning is implemented by introducing additional terms $-\lambda_i b_i^\dagger b_i$ in the model Hamiltonian.

It is worth noting that the effective interaction in Eq. (B4) can be decomposed in two terms:

$$\frac{\Gamma}{4} \sigma_x^1 \sigma_x^2 = \frac{\Gamma}{8} (\sigma_x^1 \sigma_x^2 + \sigma_y^1 \sigma_y^2) + \frac{\Gamma}{8} (\sigma_x^1 \sigma_x^2 - \sigma_y^1 \sigma_y^2) \quad (\text{B7})$$

The first term on the r.h.s. is an effective XY interaction that couples the $|10\rangle$ and $|01\rangle$ elements of the computational basis. The second term is generated by the counter-rotating contributions in the original interaction Hamiltonian, and couples the $|00\rangle$ and $|11\rangle$ components: given the large energy gap $\simeq \omega_1 + \omega_2 \gg \Gamma$ between them, this part is actually negligible. Hence, we can re-write the effective Hamiltonian as reported in the main text:

$$H_{eff} = \sum_{i=1}^2 \left(\frac{\lambda_i}{2} \sigma_z^i \right) + \frac{\Gamma}{8} (\sigma_x^1 \sigma_x^2 + \sigma_y^1 \sigma_y^2) + \text{const.} \quad (\text{B8})$$

As reported in the main text, the second term of H_{eff} is practically ineffective as far as $|\omega_1 - \omega_2| \gg \Gamma$ and it is only switched on when the two qubits are brought in resonance. In that case, the matrix form of the time-evolution operator $U_{XY}(t) = e^{-i \frac{\Gamma}{8} (\sigma_x^1 \sigma_x^2 + \sigma_y^1 \sigma_y^2) t}$ (in the computational basis $\{|00\rangle, |10\rangle, |01\rangle, |11\rangle\}$) is

$$U_{XY}(t) = \begin{pmatrix} 1 & 0 & 0 & 0 \\ 0 & \cos \frac{\Gamma t}{4} & -i \sin \frac{\Gamma t}{4} & 0 \\ 0 & -i \sin \frac{\Gamma t}{4} & \cos \frac{\Gamma t}{4} & 0 \\ 0 & 0 & 0 & 1 \end{pmatrix}, \quad (\text{B9})$$

which corresponds to the $\sqrt{\text{iSWAP}}$ gate if we choose $t = \pi/|\Gamma|$.

Appendix C: Single- and two-qubit gates

As we have pointed out in the main text, the fundamental ingredient needed to perform single and two qubit gates is the possibility to dynamically tune the oscillation frequency of the nanomechanical resonators. Here we show in full detail the protocols that are needed to obtain two specific gates, namely a single qubit x -rotation of an angle α and a two-qubit $\sqrt{\text{iSWAP}}$ gate. Unless when stated explicitly, we will assume throughout the discussion that the permanent renormalization shifts (encoded in the parameters λ_i of the main text) have already been taken into account.

We adopt a modeling similar to Ref. 10, where diagonal terms of the form

$$H_i^z(t) = V^z(t) x_i^2 = V^z(t) (b_i + b_i^\dagger)^2 \quad (\text{C1})$$

modify the oscillation frequency, while transverse components

$$H_i^{xy}(t) = V^{xy}(t) x_i = V^{xy}(t) (b_i + b_i^\dagger) \quad (\text{C2})$$

displace the equilibrium position and can be used for x - and y -rotations.

R_z -rotations can be performed by changing the qubits oscillation frequency by an amount $\delta\omega$ for a time interval δt . To implement it, a step-like pulse can be used, the temporal switching of the external fields being only limited by the response time of the control electronics (typically in the ns timescale). The resulting $H_i^z(t) = \delta\omega \Theta_{t_0}(\delta t) b_i^\dagger b_i$ will produce a phase $\phi_z = -\int dt \delta\omega \Theta_{t_0}(\delta t) = -\delta\omega \delta t$ on the $|1\rangle$ component of the basis. Here with $\Theta_{t_0}(\delta t)$ we denote a unitary step function starting at t_0 with duration δt .

As a specific example, a $R_x(\alpha)$ gate on the first nanoresonator is obtained by applying a transverse pulse

$$H_1^{xy}(t) = V^{xy}(t) x_1 = V^{xy}(t) (b_1 + b_1^\dagger) \quad (\text{C3})$$

with

$$V^{xy}(t) = A(t, t_0, \sigma) V_0^{xy} \cos(\omega_1 t). \quad (\text{C4})$$

Here V_0^{xy} denotes the amplitude scale of the pulse, while $A(t, t_0, \sigma)$ is a time-dependent modulation of the oscillatory part that describes the on/off dynamics of the gate. For example, a square pulse $A(t, t_0, \sigma) = \Theta(\sigma/2 - |t - t_0 - \sigma/2|)$ starting at t_0 and lasting for $\sigma = \alpha/V_0^{xy}$ (Θ is the unit step function) is one of the possible choices for the envelope function. Given that we are not dealing with real two-level systems, but rather trying to restrict the dynamics of a non-linear harmonic oscillator to the first two levels, the choice of the pulse profile is of great importance and can lead to significant improvement of the performances. Indeed, the frequency spectrum of a cosine-like function modulated by a square pulse may not be sufficiently narrow around the target ω_1 to avoid the activation of unwanted transitions that are close in energy, *e.g.* the $|1\rangle \leftrightarrow |2\rangle$ transition. An easy to implement but powerful tool in this context is provided by gaussian pulses, which give a fast decaying gaussian frequency spectrum. The envelope can be chosen as

$$A(t, t_0, \sigma) = e^{-\frac{(t-t_0)^2}{2\sigma^2}} \quad (\text{C5})$$

with $\sigma = \alpha/(\sqrt{2\pi} V_0^{xy})$. The gate lasts approximately $2.5\text{-}3\sigma$ on both sides of the central peak at $t = t_0$. By using gaussian pulses, the amount of non-linearity U that is required to obtain reasonably large fidelities can be reduced with respect to the square pulse case, or alternatively the strength of the tuning V_0^{xy} can be increased, thus diminishing the total gating time.

For the two-qubit gate the transmon-mediated interaction must be activated. Good isolation of the qubits during the idle phase and single-qubit gates requires that they are detuned from each other and that the transmon

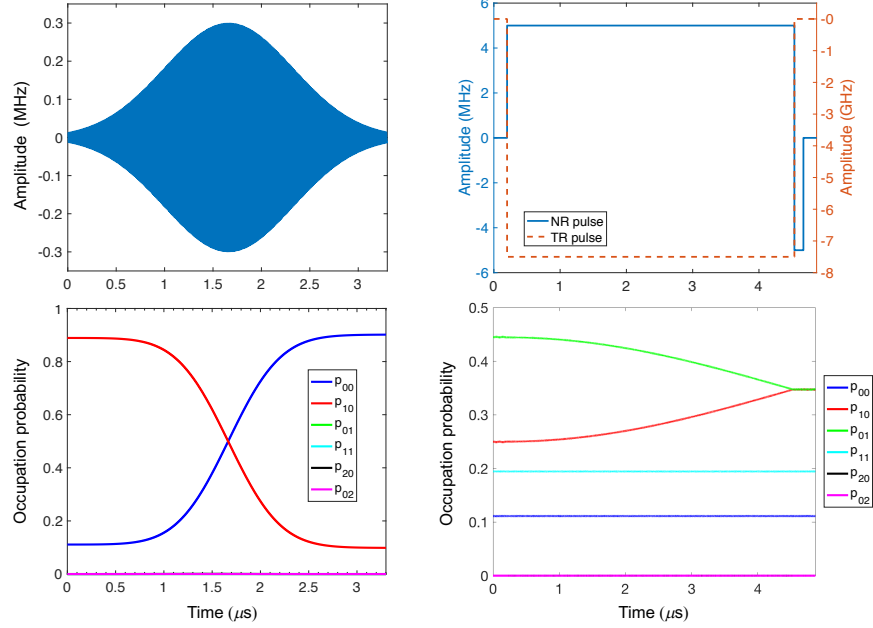


FIG. 5: Numerical simulations of single- and two-qubit quantum gates in an electromechanical circuit. Here, the system undergoes unitary evolution, with $\omega_1 = 85$ MHz and $\omega_2 = 75$ MHz. With p_{ab} we denote the component of the two-qubit wavefunction on the corresponding Fock state $p_{ab} = |\langle ab|\psi\rangle|^2$. (Bottom left) $R_x(\pi)$ rotation performed on qubit 1 while qubit 2 is kept isolated and the transmon frequency $\Omega = 10$ GHz is left unchanged. (Top Left) The gaussian oscillating pulse acting on qubit 1 needed for the $R_x(\pi)$ gate. The peak amplitude is 0.3 MHz. (Bottom right) A typical time evolution displaying a \sqrt{i} SWAP operation, with a short idle phase before and after the gate; (Top right) Frequency shifts operated on qubit 2 and on the transmon during the time evolution, including the rephasing stage on the qubit. Notice that the renormalization shift λ_2 on the qubit is not included.

is at a sufficiently high frequency (*e.g.* $\Omega \simeq 10$ GHz) to strongly suppress the residual effective coherent coupling, whose strength is

$$\Gamma = \frac{4g_1g_2\Omega(\omega_1^2 + \omega_2^2 - 2\Omega^2)}{(\Omega^2 - \omega_1^2)(\Omega^2 - \omega_2^2)} \quad (\text{C6})$$

In principle, tuning the two qubits to resonance (*e.g.* to a common intermediate frequency $\omega_r = |\omega_1 - \omega_2|/2$) is sufficient to activate coherent oscillations: the desired \sqrt{i} SWAP gate is then obtained for an interaction time $\tau = \pi/|\Gamma|$. In this case, square pulses already give good fidelities in the range of parameters that we studied. The interaction is then turned off by shifting back the frequencies of the nanoresonators, and two rephasing single qubit z -rotations are applied to correct for the additional phase accumulated by the qubits with respect to their evolution with the original bare $\omega_{1,2}$. This latter step is obtained by an inverse $-\xi_i = \omega_i - \omega_r$ pulse lasting for a time $\tau' = \text{mod}(\tau, 2\pi)$. In order to shorten the required gating time, one can exploit one peculiar property of our setup, namely the possibility of dynamically tuning the transition frequency Ω of the transmon. This is, of course, of great importance when performing long sequences in the presence of realistic dissipation processes. This shift, which is implemented in practice by varying the magnetic flux concatenated with the transmon, is essentially just another time-dependent contribution to the Hamiltonian

in the interaction picture

$$H_{TR}(t) = \delta\Omega(t) \frac{\sigma_z}{2} \quad (\text{C7})$$

Changing the frequency of the transmon affects all the effective qubit-qubit Hamiltonian parameters: in particular, reducing Ω (and thus the detuning Δ with respect to the nanoresonators) increases the coupling $\Gamma \propto g^2/\Delta$ and modifies the renormalizations λ_i . Needless to say, this procedure is limited both by the tunability range of the transmon and by the validity of the perturbative expansion in terms of g^2/Δ . Given some values of the external dissipation rates, for example, there exists an optimal $\delta\Omega$ that increases the gate fidelity without losing too much of the agreement between the actual behavior of the system and what is expected from the effective Hamiltonian description. In our protocols, we set a non zero $\delta\Omega$ during the coherent interaction time τ (which must then be computed by using $\Omega + \delta\Omega$ in equation C6) and we put the transmon back to its original frequency already during the rephasing stage. It is worth noting explicitly that when the transmon frequency is modified, the permanent shifts $-\lambda_i$ applied to the qubits must be adjusted accordingly. Figure 5 shows a single qubit $R_x(\pi)$ rotation and a two-qubit gate together with the required pulse sequences.

Appendix D: Residual thermal occupancy of nanomechanical resonators

In our analysis, we assumed that the system can be cooled at sufficiently low temperatures to safely neglect the effect of thermal interaction with the environment. Examples of ground state cooling of nanomechanical systems are already known in the literature. However, this is still a challenging issue from the experimental point of view, especially when resonators in the MHz range are considered. For this reason, we studied how the fidelities of the gates change if we add, on top of all the dissipation mechanisms that we already considered, a residual thermal interaction between the nanoresonators and the surrounding environment. Since the transmon has a much higher transition frequency (*i.e.* an higher temperature is sufficient to cool it in the ground state), we did not include thermal noise acting on this element. We used the standard Lindblad terms to model the interaction of the i -th oscillator with a bosonic thermal reservoir

$$\begin{aligned} \mathcal{L}_i[\rho] = & \frac{\chi}{2} [\bar{n}(\omega_i, T) + 1] \left(2b_i \rho b_i^\dagger - b_i^\dagger b_i \rho - \rho b_i^\dagger b_i \right) \\ & + \frac{\chi}{2} \bar{n}(\omega_i, T) \left(2b_i^\dagger \rho b_i - b_i b_i^\dagger \rho - \rho b_i b_i^\dagger \right) \end{aligned} \quad (\text{D1})$$

where ($\hbar = k_B = 1$)

$$\bar{n}(\omega_i, T) = \frac{1}{\exp\left(\frac{\omega_i}{T}\right) - 1} \quad (\text{D2})$$

In our simulations, we chose $\bar{n} = 0.1$ for both oscillators, as this generally represents a good estimate of the achievable residual thermal occupation. The rate χ can be inferred from typical line broadening of the nanoresonators, which is of the order of few tens of Hz. When average values for the other dissipation mechanism are taken into account, the effect of the residual thermal occupation is of the order of 0.01 – 0.1% of the single gate fidelity if $\chi = 50$ Hz, and of 1% if we use the very pessimistic value $\chi = 1$ kHz. The overall effect is therefore comparable to the general (zero temperature) dissipation mechanism that we included via the rates γ_i .

Appendix E: Quantum simulation of generic two-spin interactions

The time evolution $U_{XY}(t)$ induced by H_{eff} [Eq.

(B8)] can be mapped into a generic spin-spin evolution term

$$U_{\alpha\beta}(t) = e^{-iJ(\sigma_\alpha^1 \sigma_\alpha^2 + \sigma_\beta^1 \sigma_\beta^2)t}, \quad (\text{E1})$$

by properly combining it with single-qubit rotations. For instance, the following identities hold (see also Ref. 34):

$$\begin{aligned} U_{XZ}(t) &= R_x^{12}\left(\frac{\pi}{2}\right) U_{XY}(t) R_x^{12}\left(\frac{-\pi}{2}\right) \\ U_{YZ}(t) &= R_y^{12}\left(\frac{\pi}{2}\right) U_{XY}(t) R_y^{12}\left(\frac{-\pi}{2}\right) \end{aligned} \quad (\text{E2})$$

Here $R_\alpha^{12}(\theta) = \exp\left[-i\left(\frac{\sigma_\alpha^1}{2} + \frac{\sigma_\alpha^2}{2}\right)\theta\right]$ is a simultaneous rotation of both qubits by an angle θ about α axis. Another useful identity is

$$U_{XY}(t)^- = R_y^1(\pi) U_{XY}(t) R_y^1(-\pi), \quad (\text{E3})$$

with $U_{XY}^-(t) = \exp[-iJ(\sigma_x^1 \sigma_x^2 - \sigma_y^1 \sigma_y^2)t]$ and $R_\alpha^j(\theta) = \exp\left[-i\frac{\sigma_\alpha^j}{2}\theta\right]$. Note that the combination of $U_{XY}(t)$ with $U_{XY}^-(t)$ was used to simulate the Ising XX interaction reported in the main text:

$$U_{XX}(t) = U_{XY}(t) U_{XY}^-(t). \quad (\text{E4})$$

Here $U_{\alpha\alpha}(t) = \exp[-i2J\sigma_\alpha^1 \sigma_\alpha^2 t]$. The $U_{YY}(t)$ evolution can be implemented along the same lines. By combining $U_{XX}(t)$ or $U_{YY}(t)$ with a proper rotation of one of the two qubits, a generic spin-spin interaction of the form $\sigma_\alpha^1 \sigma_\beta^2$ (with $\alpha \neq \beta$) can be obtained. For instance

$$R_y^2\left(-\frac{\pi}{2}\right) U_{XX}(t) R_y^2\left(\frac{\pi}{2}\right) = e^{-i2J\sigma_x^1 \sigma_x^2 t}. \quad (\text{E5})$$

Conversely, introducing $R_y^{12}(\pi/2)$ rotations results in the operator $U_{ZZ}(t)$:

$$U_{ZZ}(t) = R_x^{12}\left(\frac{\pi}{2}\right) U_{XX}(t) R_x^{12}\left(-\frac{\pi}{2}\right). \quad (\text{E6})$$

* Electronic address: stefano.carretta@unipr.it

† Electronic address: dario.gerace@unipr.it

¹ J. Clarke and F. K. Wilhelm, *Superconducting quantum bits*, Nature (London) **453**, 1031 (2008).

² M. H. Devoret and R. J. Schoelkopf, *Superconducting Circuits for Quantum Information: An Outlook*, Science **339**,

1169 (2013).

³ J. M. Gambetta, J. M. Chow, and M. Steffen, *Building logical qubits in a superconducting quantum computing system*, npj Quant. Inf. **3**, 2 (2017).

⁴ M. Mariantoni, H. Wang, T. Yamamoto, M. Neeley, R. C. Bialczak, Y. Chen, M. Lenander, E. Lucero, A. D.

- O'Connell, D. Sank, M. Weides, J. Wenner, Y. Yin, J. Zhao, A. N. Korotkov, A. N. Cleland, and J. M. Martinis, *Implementing the Quantum von Neumann Architecture with Superconducting Circuits*, Science **334**, 61 (2011).
- ⁵ J. Koch, T. M. You, J. Gambetta, A. A. Houck, D. I. Schuster, J. Majer, A. Blais, M. H. Devoret, S. M. Girvin, and R. J. Schoelkopf, *Charge-insensitive qubit design derived from the Cooper pair box*, Phys. Rev. A **76**, 042319 (2007).
 - ⁶ C. Rigetti, J. M. Gambetta, S. Poletto, B. L. T. Plourde, J. M. Chow, A. D. Córcoles, J. A. Smolin, S. T. Merkel, J. R. Rozen, G. A. Keefe, M. B. Rothwell, M. B. Ketchen, and M. Steffen, *Superconducting qubit in a waveguide cavity with a coherence time approaching 0.1 ms*, Phys. Rev. B **86**, 100506R (2012).
 - ⁷ Z.-L. Xiang, S. Ashhab, J. Q. You, and F. Nori, *Hybrid quantum circuits: Superconducting circuits interacting with other quantum systems*, Rev. Mod. Phys. **85**, 623 (2013).
 - ⁸ S. Carretta, A. Chiesa, F. Troiani, D. Gerace, G. Amoretti, and P. Santini, *Quantum information processing with hybrid spin-photon qubit encoding*, Phys. Rev. Lett. **111**, 110501 (2013).
 - ⁹ A. Chiesa, D. Gerace, F. Troiani, G. Amoretti, P. Santini, and S. Carretta, *Robustness of quantum gates with hybrid spin-photon qubits in superconducting resonators*, Phys. Rev. A **89**, 052308 (2014).
 - ¹⁰ S. Rips and M. J. Hartmann, *Quantum information processing with nanomechanical qubits*, Phys. Rev. Lett. **110**, 120503 (2013).
 - ¹¹ J. Lozada-Vera, A. Carrillo, O. P. de Sá Neto, J. K. Moqadam, M. D. LaHaye, and M. C. de Oliveira, *Quantum simulation of the Anderson Hamiltonian with an array of coupled nanoresonators: delocalization and thermalization effects*, EPJ Quantum Technology **3**, 9 (2016).
 - ¹² M. D. LaHaye, J. Suh, P. M. Echternach, K. C. Schwab, and M. L. Roukes, *Nanomechanical measurements of a superconducting qubit*, Nature (London) **459**, 960 (2009).
 - ¹³ A. D. O'Connell, M. Hofheinz, M. Ansmann, R. C. Bialczak, M. Lenander, E. Lucero, M. Neeley, D. Sank, H. Wang, M. Weides, J. Wenner, J. M. Martinis, and A. N. Cleland, *Quantum ground state and single-phonon control of a mechanical resonator*, Nature **464**, 697 (2010).
 - ¹⁴ J.-M. Pirkkalainen, S. U. Cho, J. Li, G. S. Paraoanu, P. J. Hakonen, and M. A. Sillanpää, *Hybrid circuit cavity with a micromechanical resonator*, Nature (London) **494**, 291 (2013).
 - ¹⁵ J.-M. Pirkkalainen, S. U. Cho, F. Massel, J. Tuorila, T. T. Heikkilä, P. J. Hakonen, and M. A. Sillanpää, *Cavity optomechanics mediated by a quantum two-level system*, Nat. Comm. **6**, 6981 (2015).
 - ¹⁶ F. R. Rouxinol, Y. Hao, F. Brito, A. O. Caldeira, E. K. Irish, and M. D. LaHaye, *Measurements of nanoresonator-qubit interactions in a hybrid quantum electromechanical system*, Nanotechnology **27**, 364003 (2016).
 - ¹⁷ Y. Chu, P. Kharel, W. H. Renninger, L. D. Burkhardt, L. Frunzio, P. T. Rakich, and R. J. Schoelkopf, *Quantum acoustics with superconducting qubits*, Science **358**, 199 (2017).
 - ¹⁸ J. D. Teufel, T. Donner, D. Li, J. W. Harlow, M. S. Allman, K. Cicak, A. J. Sirois, J. D. Whittaker, K. W. Lehnert, and R. W. Simmonds, *Sideband cooling of micromechanical motion to the quantum ground state*, Nature (London) **475**, 359 (2011).
 - ¹⁹ T. A. Palomaki, J. D. Teufel, R. W. Simmonds, and K. W. Lehnert, *Entangling mechanical motion with microwave fields*, Science **342**, 710 (2013).
 - ²⁰ B. H. Schneider, V. Singh, W. J. Venstra, H. B. Meerwaldt, and G. A. Steele, *Observation of decoherence in a carbon nanotube mechanical resonator*, Nat. Comm. **5**, 5819 (2014).
 - ²¹ J. Moser, A. Eichler, J. Güttinger, M. I. Dykman, and A. Bachtold, *Nanotube mechanical resonators with quality factors of up to 5 million*, Nat. Nanotech. **9**, 1007 (2014).
 - ²² V. Singh, S. J. Bosman, B. H. Schneider, Y. M. Blanter, A. Castellanos-Gomez, and G. A. Steele, *Optomechanical coupling between a multilayer graphene mechanical resonator and a superconducting microwave cavity*, Nat. Nanotech. **9**, 820 (2014).
 - ²³ P. Weber, J. Güttinger, I. Tsioutsios, D. E. Chang, and A. Bachtold, *Coupling Graphene Mechanical Resonators to Superconducting Microwave Cavities*, Nano Letters **14**, 2854 (2014).
 - ²⁴ X. Song, M. Oksanen, J. Li, P. J. Hakonen, and M. A. Sillanpää, *Graphene optomechanics realized at microwave frequencies*, Phys. Rev. Lett. **113**, 027404 (2014).
 - ²⁵ H. W. Ch. Postma, I. Kozinsky, A. Husain, and M. L. Roukes, *Dynamic range of nanotube- and nanowire-based electromechanical systems*, Appl. Phys. Lett. **86**, 223105 (2005).
 - ²⁶ I. Kozinsky, H. W. Ch. Postma, I. Bargatin, and M. L. Roukes, *Tuning nonlinearity, dynamic range, and frequency of nanomechanical resonators*, Appl. Phys. Lett. **88**, 253101 (2006).
 - ²⁷ M. Agarwal, S. A. Chandorkar, R. N. Candler, B. Kim, M. A. Hopcroft, R. Melamud, C. M. Jha, T. W. Kenny, and B. Murmann, *Optimal drive condition for nonlinearity reduction in electrostatic microresonators*, Appl. Phys. Lett. **89**, 214105 (2006).
 - ²⁸ R. Khan, F. Massel, and T. T. Heikkilä, *Tension-induced nonlinearities of flexural modes in nanomechanical resonators*, Phys. Rev. B **87**, 235406 (2013).
 - ²⁹ S. Rips, I. Wilson-Rae, and M. J. Hartmann, *Nonlinear nanomechanical resonators for quantum optoelectromechanics*, Phys. Rev. A **89**, 013854 (2014).
 - ³⁰ R. McDermott and M. G. Vavilov, *Accurate qubit control with single flux quantum pulses*, Phys. Rev. Appl. **2**, 014007 (2014).
 - ³¹ S. Lloyd, *Universal Quantum Simulators*, Science **273**, 1073 (1996).
 - ³² I. M. Georgescu, S. Ashab and F. Nori, *Quantum Simulation*, Rev. Mod. Phys. **86**, 153 (2014).
 - ³³ A. A. Houck, H. E. Türeci and J. Koch, *On-chip quantum simulation with superconducting circuits*, Nat. Physics **8**, 292 (2012).
 - ³⁴ U. Las Heras, A. Mezzacapo, L. Lamata, S. Filipp, A. Wallraff, and E. Solano, *Digital Quantum Simulation of Spin Systems in Superconducting Circuits*, Phys. Rev. Lett. **112**, 200501 (2014).
 - ³⁵ A. Mezzacapo, U. Las Heras, J. S. Pedernales, L. DiCarlo, E. Solano, and L. Lamata, *Digital Quantum Rabi and Dicke Models in Superconducting Circuits*, Sci. Rep. **4**, 7482 (2014).
 - ³⁶ A. Chiesa, P. Santini, D. Gerace, J. Raftery, A. A. Houck, and S. Carretta, *Digital quantum simulators in a scalable architecture of hybrid spin-photon qubits*, Sci. Rep. **5**, 16036 (2015).
 - ³⁷ M. Abdi, M. Pernpeintner, R. Gross, H. Huebl, and M. J.

- Hartmann, *Quantum state engineering with circuit electromechanical three body interactions*, Phys. Rev. Lett. **114**, 173602 (2015).
- ³⁸ R. Barends, L. Lamata, J. Kelly, L. García-Alvarez, A. G. Fowler, A. Megrant, E. Jeffrey, T. C. White, D. Sank, J. Y. Mutus, B. Campbell, Yu Chen, Z. Chen, B. Chiaro, A. Dunsworth, I.-C. Hoi, C. Neill, P. J. J. O'Malley, C. Quintana, P. Roushan, A. Vainsencher, J. Wenner, E. Solano, and J. M. Martinis, *Digital quantum simulation of fermionic models with a superconducting circuit*, Nat. Comm. **6**, 7654 (2015).
- ³⁹ Y. Salathé, M. Mondal, M. Oppliger, J. Heinsoo, P. Kurpiers, A. Potočnik, A. Mezzacapo, U. Las Heras, L. Lamata, E. Solano, S. Filipp, and A. Wallraff, *Digital quantum simulation of spin models with circuit quantum electrodynamics*, Phys. Rev. X **5**, 021027 (2015).
- ⁴⁰ P. Santini, S. Carretta, F. Troiani, and G. Amoretti, *Molecular nanomagnets as quantum simulators*, Phys. Rev. Lett. **107**, 230502 (2011).
- ⁴¹ Here $\Theta_{t_0}(\delta t)$ is a step function of duration δt , starting at t_0 . In the simulations reported here, we have used pulses with a gaussian (instead of step-like) profile in order to increase spectral selectivity and hence the associated gate fidelity.
- ⁴² To complete the $\sqrt{i\text{SWAP}}$ gate one needs two additional single qubit R_z -rotations, which can be performed in parallel, to correct the additional phases $\phi_i = \xi_i \tau$ accumulated during the time τ in which the qubit frequencies were shifted by ξ_i .
- ⁴³ M. A. Nielsen and I. L. Chuang, *Quantum Computation and Quantum Information* (Cambridge University Press, Cambridge, UK, 2000).
- ⁴⁴ In all the simulations, the system is initialized in a random superposition of all the 4 states in the computational basis.
- ⁴⁵ D. Gatteschi, R. Sessoli, and J. Villain, *Molecular Nanomagnets* (Oxford University Press, New York, 2006).
- ⁴⁶ Apart from straightforward R_z rotations.
- ⁴⁷ R. A. Bari, *Classical Linear-Chain Hubbard Model: Metal-Insulator Transition*, Phys. Rev. B **7**, 4318 (1973).
- ⁴⁸ R. Somma, G. Ortiz, J. E. Gubernatis, E. Knill, and R. Laflamme, *Simulating physical phenomena by quantum networks*, Phys. Rev. A **65**, 042323 (2002).